JTTEE5 3:362-370

Solar Furnace Surface Treatment of Plasma-Sprayed Thermal Barrier Coatings

A. Ferriere, L. Lestrade, A. Rouanet, A. Denoirjean, A. Grimaud, and P. Fauchais

An original process of superficial thermal treatment is described. This process has been successfully applied to partially stabilized yttria-zirconia coatings (ZrO_2-Y_2O_3) to increase the lifetime of the thermal barriers. A thin superficial layer was melted, and morphological transformations were observed. A microstructural comparison between as-sprayed layers and thermally treated layers is presented.

1. Introduction

PLASMA-SPRAYED thermal barrier coatings have been applied successfully to vanes in the high-pressure stage and combustion chamber of aircraft engines. Beyond increasing the lifetime of the coated metallic part, the principal advantage of such coatings is higher reactor efficiency resulting from the slight increase of the combustion temperature and from the reduced flow requirement for blade cooling air (Ref 1).

Yttria-stabilized zirconia (from 6 to 30 wt% of Y_2O_3) is considered one of the best ceramics for thermal barriers for aircraft engines (Ref 2-5). The plasma spraying process is widely used to make these coatings, because the relatively high porosity (≈10%) enhances the thermal barrier effect.

The service conditions, especially the thermal cycling, of thermal barriers cause severe damage that reduces barrier lifetime. Spalling of the coating results when the hot oxidizing gases penetrate into the coating through connected cracks and macropores and then attack the substrate/coating interface (Ref 6).

The aim of superficial thermal treatments is to seal the pores at the surface of the plasma-sprayed ceramic layer. In addition, the possibility of obtaining a smooth surface, and thus good aerodynamic qualities, is of particular interest for vane coatings.

The published studies on superficial thermal treatments primarily relate to laser surfacing (Ref 7-9). Jasim et al. (Ref 8), for example, studied laser-induced superficial melting of a plasma-sprayed coating made of yttria-stabilized zirconia with a high percentage (30 wt%) of Y_2O_3. Smurov et al. (Ref 9) have begun studies to optimize the laser treatment of duplex-type ZrO_2-CeO_2-Y_2O_3 thermal barriers. The superficial modifications obtained in this latter case appear to meet technical requirements.

The solar furnace has been successfully used to perform superficial thermal treatment in the field of high-temperature metallurgy (Ref 10, 11). The spatial distribution range and the heat flux level can be easily controlled for monitored irradiation. This has prompted study of the superficial thermal treatment of plasma-sprayed thermal barriers using a solar furnace (Ref 11, 12). The feasibility of this type of treatment has been established from a theoretical point of view (Ref 12).

This paper presents the results of a feasibility study made at IMP-Odeillo. The ceramic layers were made of partially stabilized yttria-zirconia with 7.6 wt% Y_2O_3 (4.3 mol% Y_2O_3), plasma sprayed onto a cast iron substrate. Characteristics of the base material and the plasma spraying parameters are briefly outlined. Then the process of superficial thermal treatment in a solar furnace is presented, along with studies of its effect on plasma-sprayed layer properties. Thermomechanical properties of the coatings before and after thermal treatment are then compared.

Keywords microstructure, partially stabilized zirconia, postprocessing, solar furnace treatment, surface treatment

A. Ferriere, L. Lestrade, and **A. Rouanet,** Institut de Science et de Génie des Matériaux et des Procédés, Odeillo 66125, France; **A. Denoirjean, A. Grimaud,** and **P. Fauchais,** Laboratoire de Matériaux Céramiques et Traitements de Surface, URA 320 CNRS, Université de Limoges, Limoges 87060, France.

2. Description

The chemical composition of the basic product before spraying is given in Table 1. The particle size of this fused and crushed powder was –45 +22.5 μm (less than 5 wt% of particles have a diameter greater than 45 μm and less than 5% of particles have a diameter smaller than 22.5 μm).

The substrates were made of cast iron FT 25, which has a thermal expansion coefficient ($\alpha \cong 10^{-6}\,K^{-1}$) close to that of the zirconia coatings. Disk shaped substrates were 5 mm thick and 12 or 26 mm in diameter. Prior to spraying, substrates were grit blasted with a pressure type machine with white alumina (mean grit size 1.2 mm, blasting distance 100 mm, nozzle orthogonal to the substrate, nozzle internal diameter 8.6 mm, sand blasting pressure 0.6 MPa, blasting time 5 sec) with a resulting RA of 13 μm. The blasted substrates were cleaned in acetone in an ultrasonic bath.

Table 1 Powder composition before spraying

Component	Weight percent
ZrO_2	91.92
Y_2O_3	7.60
SiO_2	0.16
Fe_2O_3	0.13
Al_2O_3	0.11
TiO_2	0.08

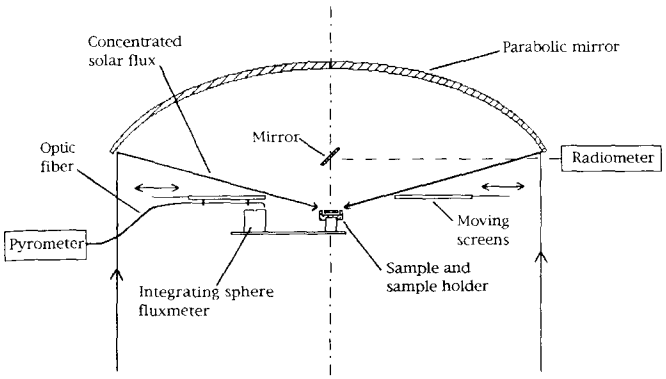

Fig. 1 Experimental setup

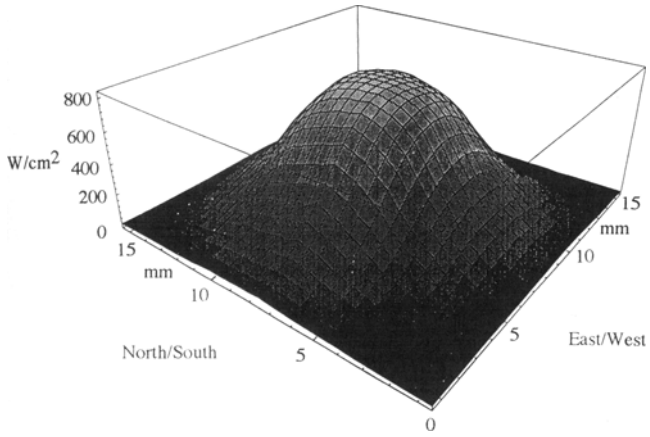

Fig. 2 Distribution of the irradiation intensity in the focal plane

The disks were mounted onto a cylindrical holder 110 mm in diameter. The torch was pointed at 90° to the cylinder surface and moved parallel to the cylinder axis. The laboratory had manufactured the torch. The torch nozzle orifice diameter was 7 mm and the powder was injected at 90° to the plasma jet axis 3 mm upstream of the nozzle exit with an internal injector tube 1.8 mm ID.

The holder and the disks were cooled down by 3 compressed air jets blown through slits with a section of 1×28 mm^2 onto the cylinder face facing the plasma torch. The surface temperature was controlled by a monochromatic infrared pyrometer ($\lambda = 5.2$, $\Delta\lambda = 1.2$ nm) with a preliminary calibration based on the emissivities of the blasted substrate and of the coated one.

The substrates were preheated by the plasma jet at the standoff distance, using the spraying parameters reported in table 2. The preheating time was 180 s and the surface temperature was adjusted to 300 °C, with a temperature deviation of ±20 °C, by controlling the air flowrate in the cooling slits. Such preheating increased the wettability of surface by the impacting molten droplets Ref 13. The interface contact was improved and, consequently, the adhesion was increased Ref 14.

The powder mass flow rate was 1 kg/h and, under these spraying conditions with substrate preheating at 300 °C and a deposition efficiency of 55%, the powder injection resulted in an increase of about 40 °C in the surface temperature. A smooth cooling down of the coating and substrate holder after spraying

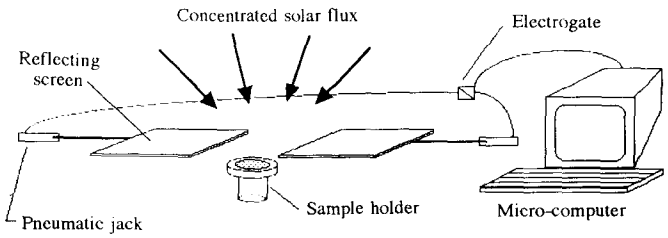

Fig. 3 Irradiation duration control system

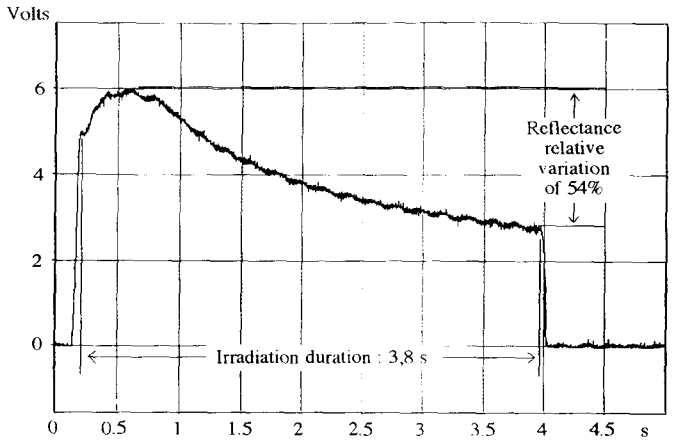

Fig. 4 Normal monochromatic reflected flux measured during irradiation

Table 2 Spraying parameters

Plasma gas flow rates (slm)	Ar : 36 - H_2 : 12
Current intensity (A)	575
Voltage (V)	68
Powder carrier gas flow rate (slm)	4
Injector i.d. and position upstream of the nozzle exit (mm)	1.8 and 3
Spraying distance (mm)	100
Rotating velocity (rpm) - torch speed (mm/s)	180 - 24
Coating thickness (μm)	350-400

was obtained by shutting off simultaneously the power source and the cooling air jets while the holder was kept rotating. With this procedure, 200 s were necessary to obtain a coating at room temperature.

3. Solar Furnace Heat Treatment

3.1 *Experimental Setup*

The solar concentrator was parabolic, with a focal length of 85 cm (Fig. 1). The available power reached 2 kW when the incident solar flux on the heliostat was 10 MW/m^2. In this case, the maximum concentrated flux at the focal point was about 12 MW/m^2. This power density, two orders of magnitude smaller than that of lasers, allowed most of the refractory oxides (diameter, 5 mm; thickness, 0.5 mm) to be melted in a few seconds.

The distribution of the radiation intensity (Fig. 2) was measured at the focal plane using a fluxmeter (photoelectrical detector) coupled with an integration sphere. The spatial resolution of

this device was 0.5 mm. It was calibrated using a reference calorimeter.

The solar flux was 7.70 MW/m^2 when the measurements were performed, resulting in a maximum concentrated flux of 9.3 MW/m^2. The spatial flux distribution was always higher than 90% of its maximum value on an average surface of 20 mm^2.

The shutter was made of two reflecting screens sliding horizontally. They were moved by two pneumatic jacks simultaneously driven by an electrogate monitored by a microcomputer. These two small, uncooled screens intercepted the concentrated solar flux 5 cm above the focal plane (Fig. 3).

3.2 *Measurements*

The position of the focal point and available flux were determined using the fluxmeter. A monochromatic radiometer (0.65 μm) measured, in the normal direction, the variation of the flux reflected by the irradiated surface. In this way, the irradiation duration and the evolution of the absorbed flux by the treated surface were controlled.

A two-color pyrometer (λ_1 = 1.3 μm, λ_2 = 1.5 μm) developed at IMP-Odeillo was used to measure temperature evolution during cooling of the irradiated surface. At the end of the irradiation, an optical fiber fixed to one of the reflecting screens targeted the center of the treated surface. The distance between this surface and the fiber tip was about 1 mm, resulting in a temperature measurement area smaller than 1 mm in diameter. A fast data acquisition system (1000 Hz), connected to a microcomputer, collected the data during the heat treatment.

4. Results

Coating surface melting was achieved with a maximum concentrated flux of 9.3 MW/m^2 for three 12 mm diam samples with a coating thickness of 400 μm. The exposure durations, the melted depths, and the diameter of the melted area are given in Table 3.

The results of the heat treatments were very similar, with only the dimensions of the melted area differing.

Figure 4 shows the variation of the flux reflected by the irradiated surface of the sample treated for 3.8 s. Both screen open-

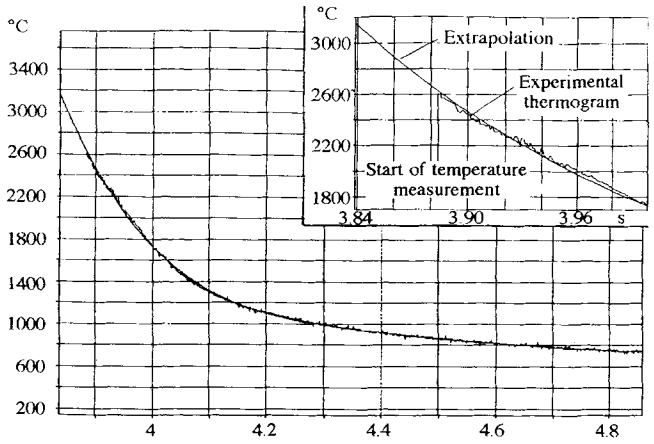

Fig. 5 Temperature measurement during cooling

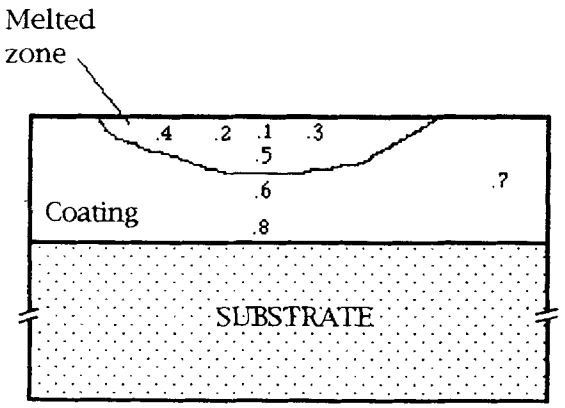

Fig. 6 Chemical composition of the 3.8 s sample at various locations of the coating as measured by microprobe analysis

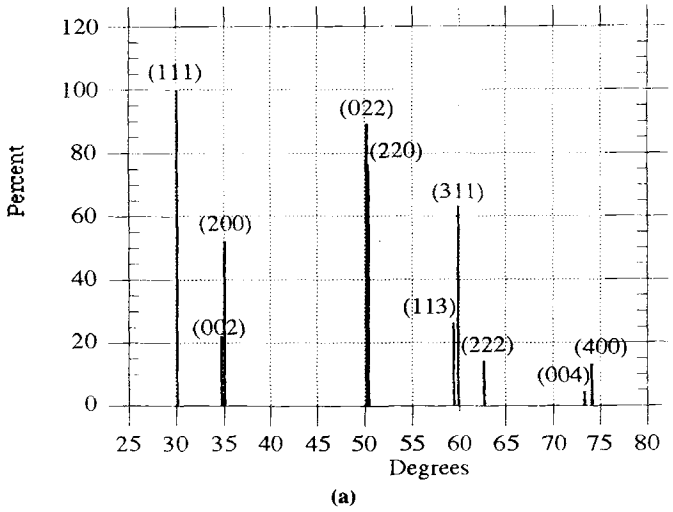

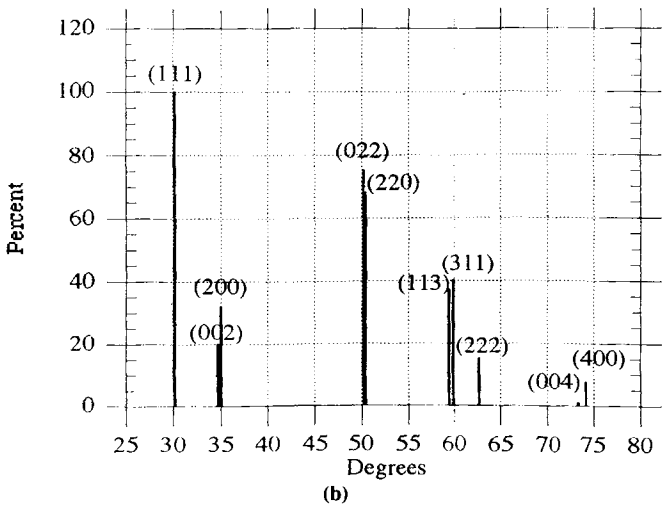

Fig. 7 X-ray diffraction patterns. (a) As-sprayed coating. (b) Treated coating

ing and shutting durations were 40 ms—very short times compared to the irradiation time.

The monochromatic absorption varied in a ratio of 53% during the heat treatment. It was assumed that these variations of optical properties were due to a modification of chemical bonds at the coating surface.

Measurement of the surface temperature evolution was not valid until the screens were completely shut and only the cooling of the treated surface was measured (Fig. 5). The cooling rate during solidification governed to a great extent the crystalline structure of the treated ceramic layer. This cooling rate was estimated from the temperature measurements to better understand the treated coating microstructure.

The temperature, of course, was maximum at the end of irradiation. To determine this maximum, the measured temperature was extrapolated to the time at which the screen shutting began. The maximum temperature estimated from Fig. 5 was 3000 °C,

Table 3 Experimental parameters

Irradiation duration, s	Depth of the melted layer, μm	Diameter of the melted area, mm
3	...	3 ± 0.5
3.5	70 ± 10	6 ± 0.5
3.8	90 ± 10	8 ± 0.5

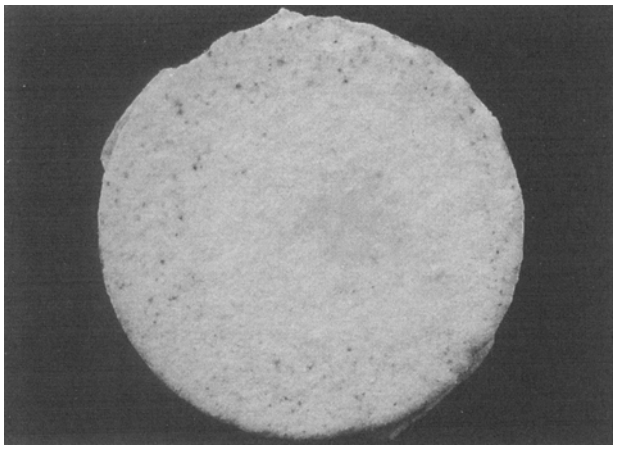

Fig. 8 Treated surface (irradiation duration of 3 s)

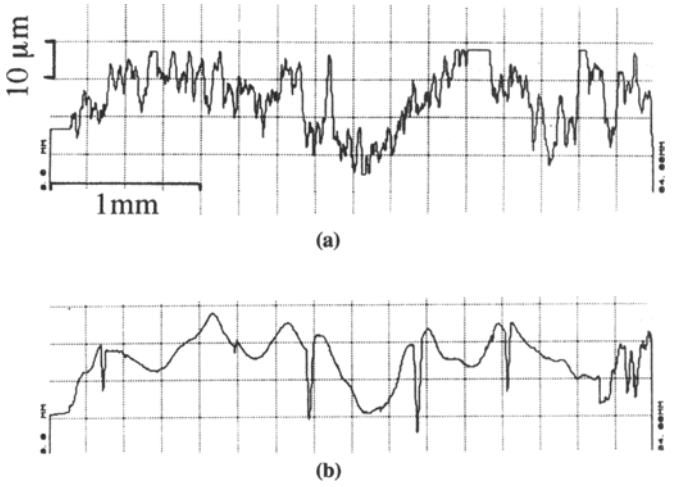

Fig. 9 Roughness profiles before (a) and after (b) heat treatment

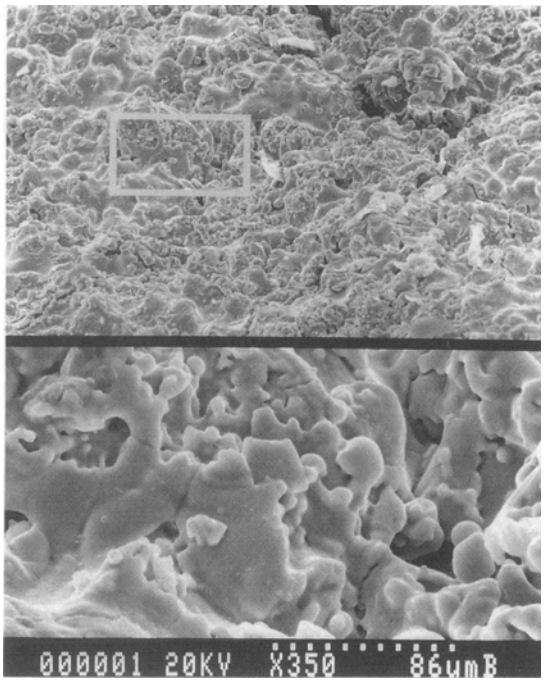

(a)

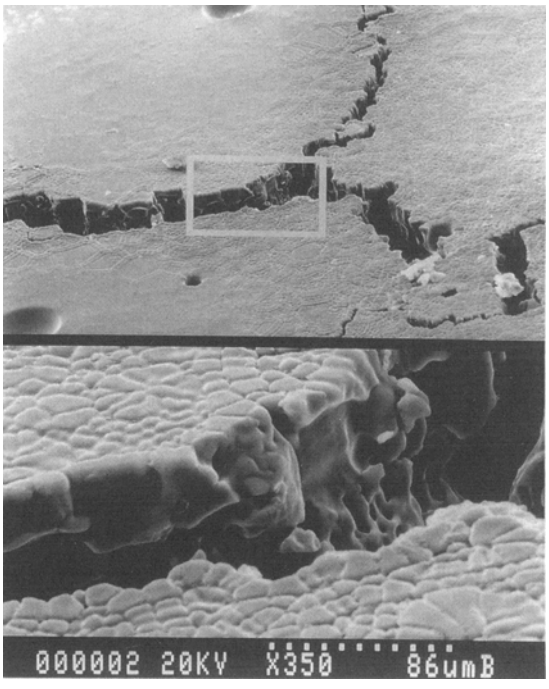

(b)

Fig. 10 (a) As-sprayed coating surface. (b) Heat-treated surface

assuming, perhaps in an oversimplified manner, that the temperature of the liquid phase was not homogenized by convective motions. In this case, the maximum calculated cooling rate was about 12,000 K/s.

5. Comparative Microscopic Characterization of Thermal Barriers before and after Surface Heat Treatment

Neither the substrate nor the ceramic/substrate interface was altered by the heat treatment. The thickness of the affected layer never exceeded 100 μm.

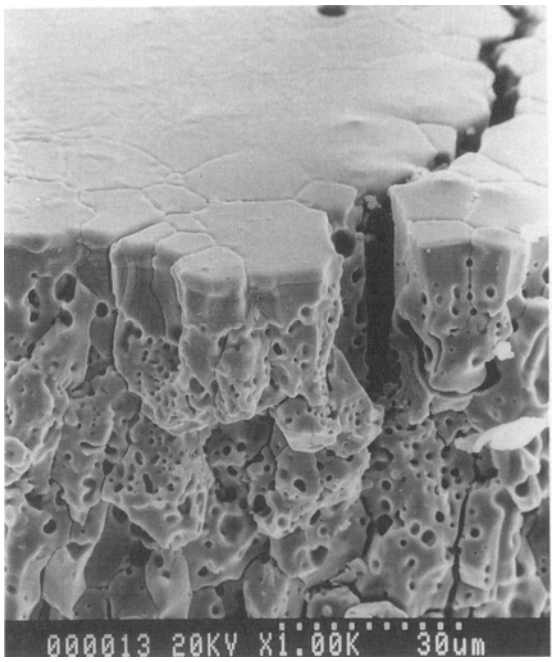

Fig. 11 Surface and fracture surface of the treated layer

5.1 *Chemical Composition*

Microprobe analysis, especially when examining the amounts of zirconium, yttrium, and oxygen, revealed that the Y_2O_3 percentage in the melted zone was the same as that in the as-sprayed coating (7.6 wt%). The analyzed points are shown in Fig. 6; Table 4 gives the weight percentages.

5.2 *Crystalline Structure*

The x-ray diffraction spectra of the melted area present the same diffraction pattern as that of the as-sprayed coating, with a predominant tetragonal phase (Fig. 7). The Y_2O_3 percentage in the melted layer is still 7.6 wt%. Recrystallization after surface melting occurred in a metastable tetragonal phase, rich in Y_2O_3, called <t'> (Ref 5). Because the return to the equilibrium mixture of <c> + <t> is very slow, the mechanical durability of this material is expected to be good. After melting, the cooling rate was sufficiently fast (greater than 10^4 K/s) to quench the <t'> phase. The ratio c/a = 1.010 is the same as that of the as-sprayed coating lattice.

No noticeable difference in the crystalline structure of the yttria-zirconia was seen before or after heat treatment. It is thus reasonable to assume that the mechanical resistance of the heat-treated zone is similar to that of the as-sprayed coating.

5.3 *Morphology*

The numerous and significant morphological transformations observed in the superficial layer of the thermal barrier coating after the solar treatment demonstrate the efficiency of this process.

5.3.1 Surface Conditions

Figure 8 shows the surface of the 3 s irradiated sample. The treated zone is pale yellow, whereas the untreated surface is pale gray. The unmelted corona is more pale than the as-sprayed coating. These modifications probably result from a small variation in the surface chemical composition, relative to the oxygen amount in zirconia. However, the microprobe resolution is not

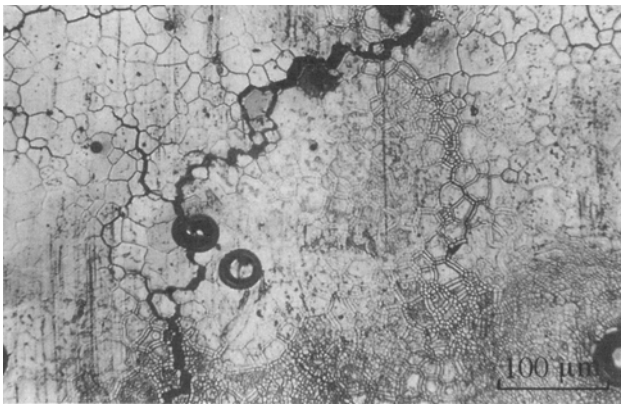

(a)

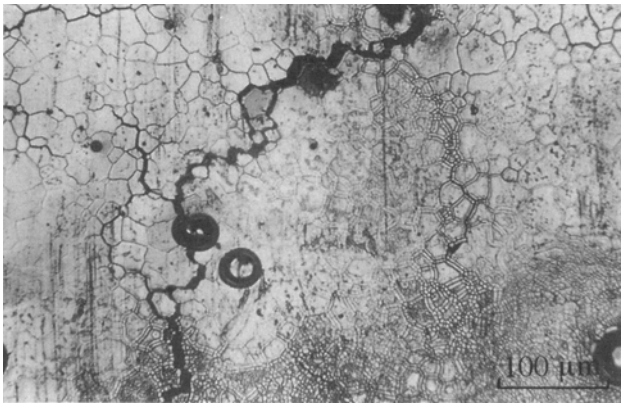

(b)

Fig. 12 Central zone (a) and peripheral zone (b) of the treated area

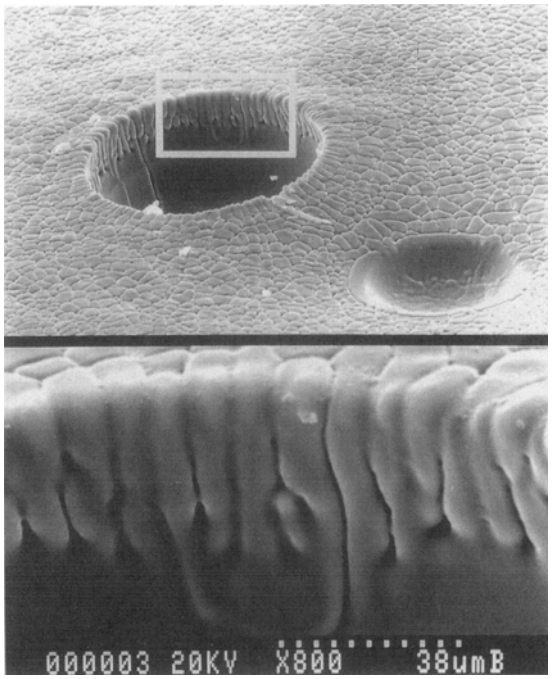

Fig. 13 Craters in the treated layer

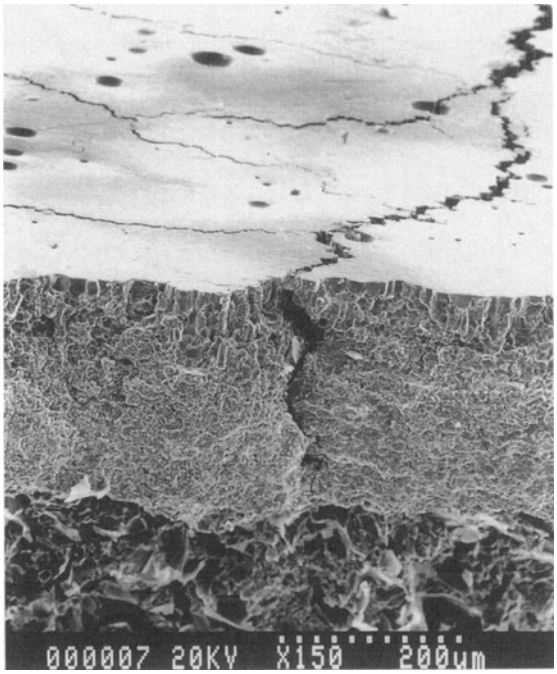

Fig. 15 Fracture surface of a crack in the treated layer

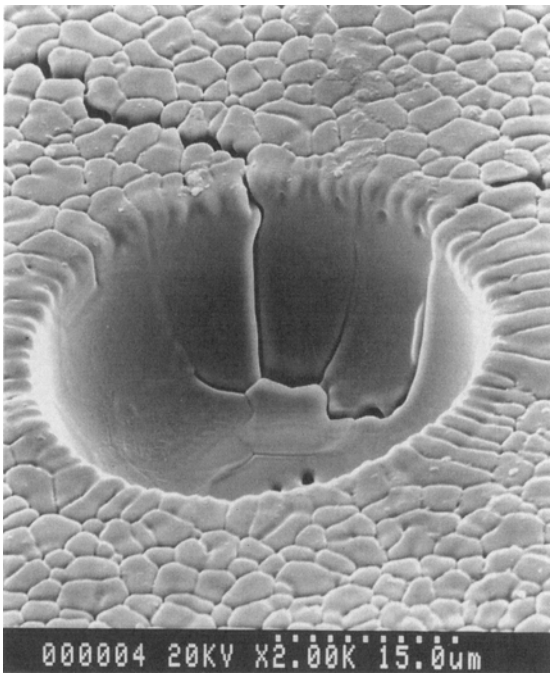

Fig. 14 Fracture surface of a bubble near the free surface

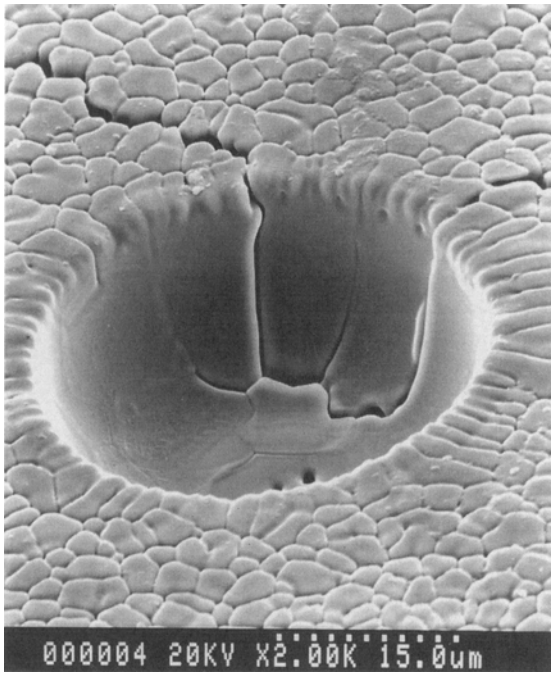

Fig. 16 Microcracked crater

Table 4 Weight percentages of oxygen, zirconium, and yttrium

	Position								
Element	**1**	**2**	**3**	**4**	**5**	**6**	**7**	**8**	**Feedstock**
Oxygen	25.8	27.2	27.2	26.9	27.7	27.7	26.7	28.3	25.36
Zirconium	64.7	63.2	63.2	63.7	63.4	64.2	63.1	65.0	64.33
Yttrium	9.6	9.3	11.2	9.0	10.2	9.6	10.0	10.3	10.31

accurate enough to detect such variations occurring in a very thin layer (~1 μm).

The rough surface of the as-sprayed coating became smoother after melting and solidification. The arithmetical average roughness decreased from 4.1 to 2.8 μm. The difference in roughness between the as-sprayed layer and the melted layer is shown in Fig. 9.

The heat-treated surface comprises cells, craters, cracks, and microcracks (Fig. 10b). Its appearance is quite different from that of the untreated surface (Fig. 10a). The cells, varying between 1 and 50 μm in size, were separated by small holes (5 to 10 μm deep), which are preferential sites for crack initiation (Fig. 11). The formation of such cells is due to a localized variation in the chemical composition or concentration of impurities (Ref 14). The slight change in color observed could be connected with this mechanism. The formation of cells on laser-sealed surfaces was also reported by Jasim et al. (Ref 8). However, the connection between cell size and laser flux density is contrary to that observed in the case of solar treatment. In this case, cell size (Fig. 12) decreased with increasing solar flux density; that is, the cells in the central area of the treated sample, which received a higher thermal flux, were smaller (1 μm) than those in the peripheral part, which received a lower flux.

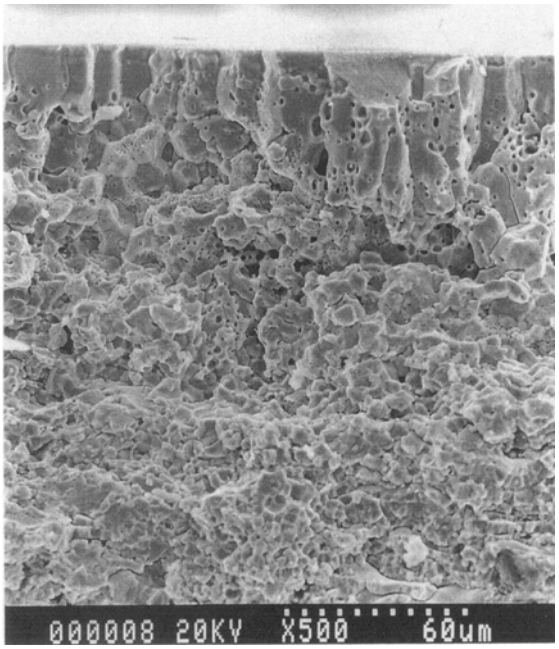

Fig. 17 Fracture surface of the treated layer

The number of craters (Fig. 13) increased with increasing flux density. The fracture surface exhibited bubbles near the free surface (Fig. 14) of about the same diameter as the craters (5 to 10 μm). Bubbles and craters are produced by the release of gas trapped in pores and by the ascending movement of bubbles in the liquid phase. This mechanism reduced porosity and was also reported by Smurov et al. (Ref 9) for the case of laser treatments.

In the treated zone, crack depth was about 30 μm, with an average width of 5 μm. Some of the wider and deeper cracks reached the coating/substrate interface (Fig. 15). Some craters were themselves microcracked (Fig. 16). The cracks and microcracks appeared at the end of the solidification process when high mechanical stresses were applied to the solid phase near the solidification front. Such stresses were a consequence of the volume variation during solidification and were caused by the density mismatch between the liquid and the solid phases.

5.3.2 Layer Morphology

The fracture surface of the thermal barrier coating treated in a solar furnace (Fig. 15 and 17) revealed the presence of three layers with different thicknesses and morphologies. No spalling was observed. The treated barrier exhibited very good cohesion, as indicated by the cross section shown in Fig. 18.

The structure of the as-sprayed coating—a buildup of lenticular, flattened particles— is shown in Fig. 19; the deepest layer was unaffected by the heat treatment. Interstitial and lacu-

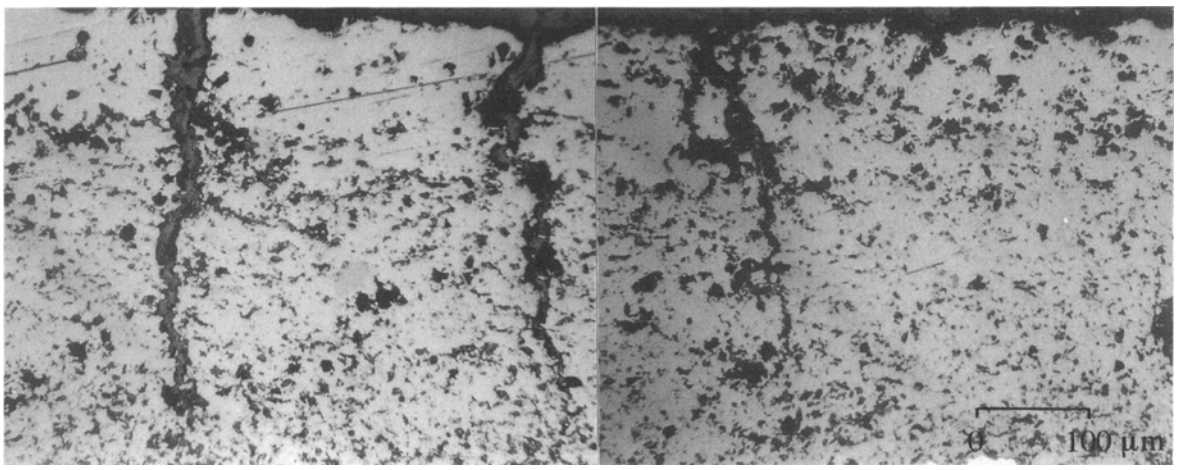

Fig. 18 Cross section of the treated layer

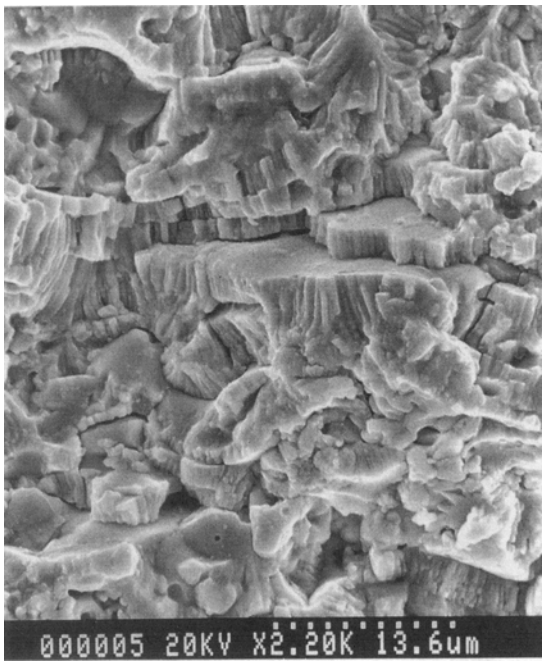

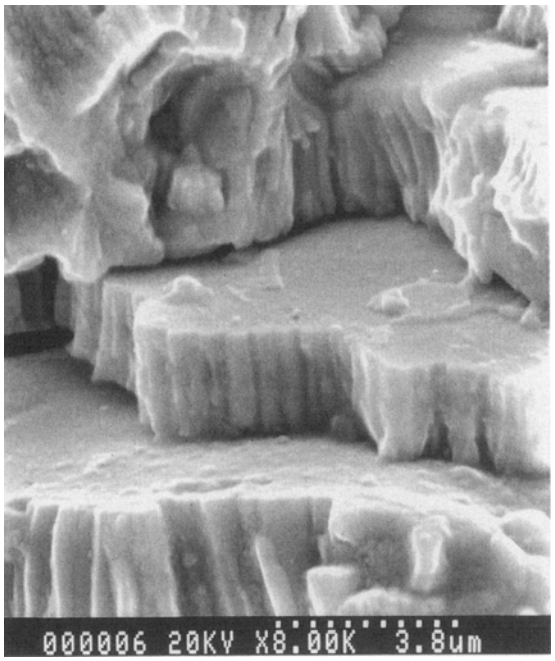

Fig. 19 Fracture surface of the deep, untreated layer

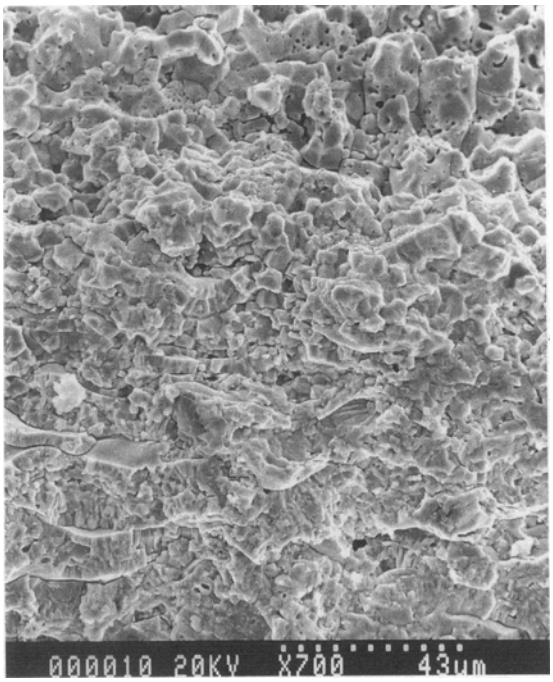

Fig. 20 Fracture surface of the intermediate layer

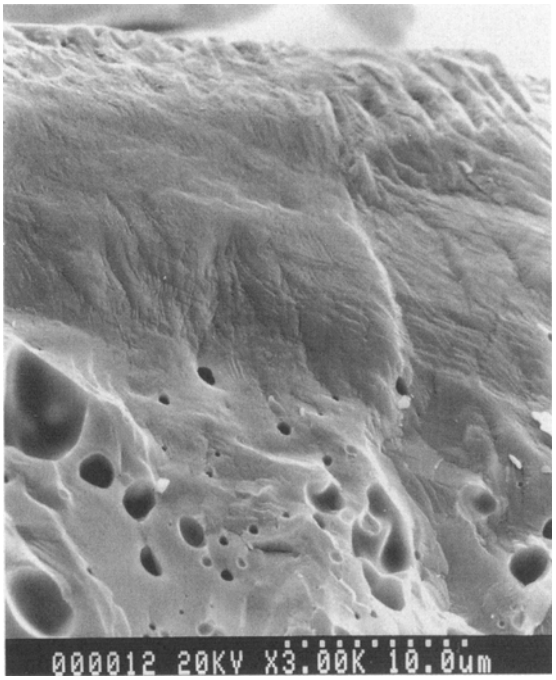

Fig. 21 Fracture surface of the superficial melted layer

nar porosity with a lamellar geometry and a small amount of micropores and microcracks parallel to the columnar grains were evident.

The intermediate layer was 20 μm thick and exhibited a typical transition morphology (Fig. 20). The structure shifted from a splat morphology to a pile of fragments. The pore size was smaller than that of the unaffected zone. In this intermediate layer, the effect of heat treatment applied to the coating surface was similar to that of sintering after extended annealing times (Ref 4).

Lastly, the morphology of the melted and recrystallized heat-treated layer was very dense (Fig. 11 and 21). The residual porosity was spherical, and pores became micropores—a morphology quite typical of molten and rapidly cooled materials.

rosity was spherical, and pores became micropores—a morphology quite typical of molten and rapidly cooled materials.

6. Conclusions

The morphological transformations described in this paper are consequences of the mechanisms that occur in the thermal barrier during solar furnace heat treatment. The melting released porosity, with a volume decrease of the material. Microbubbles gathered in the liquid phase and then moved to the free surface. Even when solidification was very fast (10^4 K/s), the solidification front moved from the free surface to the substrate. The shaped crust was smooth, but with a residual cellular relief, and was covered with craters. The outer layer contained bubbles. When the heart solidified, stresses caused superficial microcracks and cracks in the melted layer, with some cracks reaching the coating/substrate interface. No spalling was observed after the treatment.

The feasibility of solar furnace heat treatment of plasma-sprayed thermal barrier coatings was established from an experimental point of view. Coatings of zirconia partially stabilized with yttria (7.6 wt% Y_2O_3) sprayed onto cast iron with no underlayer were tested. These as-sprayed coatings exhibited microstructural and morphological features typical of thermally sprayed materials.

The desired sealing effect by melting a thin layer was obtained without rupture or spalling of the thermal barrier. The process was reproducible and led to solidification conditions, which implied no modification either of the ceramic chemical composition or of the crystalline structure. The surface condition was smooth and cellular, but cracked. Most cracks were superficial; however, in the highly irradiated zone, some were deep, wide, and reached the coating/substrate interface. This could lead to substrate oxidation if the thermal barrier was used in severe conditions, such as those encountered in gas or aeroengine turbines.

Comparative studies of as-sprayed and heat-treated coatings should be extended to optical surface properties, mechanical stress characterization, and thermal cycling resistance using coatings sprayed on superalloys with an underlayer.

In this preliminary study, the solar furnace heat treatment was limited to the surface covered by the concentrator beam in the focal plane. The next step will involve moving the sample according to a given pattern, which offers these advantages:

- Treatment of a larger area with easy control of irradiation duration
- Decrease in the mechanical stresses generated during the solidification process by changing the solidification front geometry

It is expected that the melting of a very thin layer will reduce the number and depth of cracks.

References

1. C.H. Liebert and R.A. Miller, Ceramic Thermal Barrier Coatings, *Ind. Eng. Chem. Prod. Res. Dev.*, Vol 23, 1984, p 344-349
2. J.W. Fairbanks and R.J. Hecht, The Durability and Performance of Coating in Gas Turbine and Diesel Engines, *Mater. Sci. Eng.*, Vol A120, 1989, p 13-24
3. R. McPherson, A Review of Microstructure and Properties of Plasma Sprayed Ceramic Coatings, *Surf. Coat. Technol.*, Vol 39/40, 1989, p 173-181
4. H.E. Eaton and R.C. Novak, Sintering Studies of Plasma-Sprayed Zirconia, *Surf. Coat. Technol.*, Vol 32, 1987, p 227-236
5. D.S. Suhr, T.E. Mitchell, and R.J. Keller, Microstructure and Durability of Zirconia Thermal Barrier Coatings, *Adv. Ceram. Sci. Technol. Zirconia II*, Vol 12, 1984, p 503-517
6. R.A. Miller and C.E. Lowel, Failure Mechanisms of Thermal Barrier Coatings Exposed to Elevated Temperatures, *Thin Solid Films*, Vol 95, 1982, p 265-273
7. A. Ferriere, G. Flamant, J.F. Robert, P. Pekshev, I. Smurov, and A. Chistyi, Characterisation of As-Sprayed and Laser-Treated Zirconia-Based Plasma-Sprayed Coatings, *Coll. Phys.*, Vol C5, 1990, p 393-402
8. K.M. Jasim, R.D. Rawlings, and D.R.F. West, Characterization of Plasma Sprayed Layers of Fully Yttria-Stabilized Zirconia Modified by Laser Sealing, *Surf. Coat. Technol.*, Vol 53, 1992, p 75-86
9. I. Smurov, A. Uglov, Y.U. Krivonogov, S. Strulese, and C. Bartuli, Pulsed Laser Treatment of Plasma-Sprayed Thermal Barrier Coating: Effects of Pulse Duration and Energy Input, *J. Mater. Sci.*, Vol 27, 1992, p 4523-4530
10. G.P. Rodriguez, V. Lopez, J.J. De Damborenea, and A.J. Vasquez, Surface Transformation Hardening on Steels Treated with Solar Energy in Central Tower and Heliostat Field Installation, *6th Int. Symp. Solar Thermal Concentrating Technologies* (Mojacar, Spain), CIEMAT, Madrid, 1992
11. J.T. Stanley, C.L. Fields, and J.R. Pitts, Traitements de Surfaces par des Faisceaux de Rayons Solaires, *Traite. Therm.*, Vol 248, 1991, p 47-52 (in French)
12. A. Ferriere, G. Flamant, G. Olalde, and I. Smurov, Qualification au four Solaire de Barrières Thermiques à Base de Céramiques Déposées par Plasma, *High Temp. Chem. Process.*, Vol 1, 1992, p 211-228 (in French)
13. M. Mellali, M. Vardelle, A. Grimaud, and P. Fauchais, Influence of the Temperature Substrate Monitoring on the Adhesion-Cohesion of Alumina Plasma Sprayed Coating, *International Thermal Spraying Conference*, German Welding Society, Dusseldorf, 1993, p 392-394
14. B. Chalmers, *Principles of Solidification*, John Wiley & Sons, 1964, chap. 5